# Quantum and quasi-classical calculations for the $S^+ + H_2(v,j) \rightarrow SH^+(v',j') + H$ reactive collisions

Alexandre Zanchet* and Octavio Roncero
*Instituto de Física Fundamental, CSIC, C/ Serrano, 123, 28006 Madrid, Spain.*

Niyazi Bulut
*Dept. of Physics, Firat University, Elazig, Turkey*

(Dated: March 16, 2016)

State-to-state cross sections for the $S^+ + H_2(v,j) \rightarrow SH^+(v',j') + H$ endothermic reaction are obtained with quantum wave packet(WP) and quasi-classical (QCT) methods for different initial ro-vibrational $H_2(v,j)$ over a wide range of translation energies. Final state distribution as a function of the initial quantum number is obtained and discussed. Additionally, the effect of the internal excitation of $H_2$ on the reactivity is carefully studied. It appears that energy transfer among modes is very inefficient, that vibrational energy is the most favorable for reaction and rotational excitation significantly enhance reactivity when vibrational energy is sufficient to reach the product. Special attention is also paid on an unusual discrepancy between classical and quantum dynamics for low rotational levels while agreement improves with rotational excitation of $H_2$, An interesting resonant behaviour found in WP calculations is also discussed and is associated to the existence of roaming classical trajectories that enhance the reactivity of the title reaction. Finally, a comparison with the experimental results of Stowe *et al.*[1] for $S^+$+ HD and $S^+$+$D_2$ reactions, finding a reasonably good agreement with those results.

## I. INTRODUCTION

Sulfur is one of the most abundant elements in space, after H, He, O, C and N. Its relative abundance with respect to H is $10^{-5}$. However, the relative abundance of all the sulfur containing molecules detected so far in space is several order of magnitudes lower. Sulfur has not being detected in ices in space, and it is therefore concluded that it must be present in highly refractive grains, not yet determined[2, 3].

The first step in the sulfur chemistry is the formation of its hydride, in neutral or cationic form. $SH^+$ can be formed in collisions of atomic S with $H_3^+$, but $H_3^+$ ion is only abundant in cold molecular clouds. The recent detection of $SH^+$ in hot regions, such as star formation regions[4], diffuse clouds[5, 6], and dense PDRs[7], indicates that there must by other routes to form this hydride cation. This low rotational N=1 $\rightarrow$ 0 transition of $SH^+(^3\Sigma^-)$ was recently measured in the laboratory by Halfen and Ziurys[8].

One possible pathway is the

$$S^+ + H_2 \rightarrow SH^+ + H \tag{1}$$

reaction. This reaction is endothermic for $H_2(v=0)$ by $\approx 0.86$ eV[1, 9], but it may be the source of $SH^+$ when considering vibrationally excited states of $H_2(v \geq 2)$, as proposed by Agundez *et al.*[10].

Very recently, a potential energy surface (PES) for the ground quartet electronic state of this system has been calculated, and reaction rate constants were obtained using a quasi-classical trajectory (QCT) method[11]. The rates obtained increase substantially with increasing the initial vibrational state of $H_2$, and were used to model

*Electronic address: alexandre.zanchet@csic.es

$SH^+$ fractional abundance as a function of the visual extinction, $A_v$. For $A_v < 3$, there is a notorious increase of the abundance of $SH^+$ because at these high UV fluxes there is a relatively high abundance of vibrational excited $H_2$. At $A_v > 4$, however, the reaction of S with $H_3^+$ is the dominant route for the formation of $SH^+$. The reaction of Eq. (1) is therefore expected to play an important role in the illuminated regions of photodissociation regions (PDR).

The aim of this work is to understand the effect of initial internal energy of $H_2$, and to compare QCT with quantum calculations to check their validity. In addition, we study the state-to-state dynamics, to provide state-to-state cross sections to be used to determine the emission from excited rotational states, as recently done for $CH^+$[12] and $OH^+$[13].

The paper is organized as follows. Section II briefly describes the details of the QCT methods and of the quantum wave packet (WP) used in this work. Section III describes the results obtained and discuss the differences between quantum and classical results. Finally, section IV is devoted to extract some conclusions.

## II. METHODOLOGY

### A. Quasi-classical calculations

The QCT total reaction cross section is calculated as

$$\sigma_{vj}(E) = \pi b_{max}^2 P_r(E) \quad \text{with} \quad P_r(E) = \frac{N_r}{N_{tot}}, \qquad (2)$$

where $N_t$ is the maximum number of trajectories with initial impact parameter lower than $b_{max}$, the maximum impact parameter for which reaction takes place, and $N_r$ is the number of trajectories leading to $SH^+$ products. The QCT calculations have been performed using the code miQCT described previously[14]. The Hamilton equations are integrated using a step adaptive Adams-Bashforth-Moulton Predictor-corrector method[15], using the two Jacobi vectors $\mathbf{r}$ and $\mathbf{R}$ in cartesian coordinates and their generalized momenta, where $\mathbf{r}$ is the vector connecting the two hydrogens and $\mathbf{R}$ is the vector connecting the center of mass of $H_2$ and $S^+$. To calculate the total integral cross section of Eq. (2), a Monte Carlo sampling of initial conditions is done following the method of Karplus and co-workers[16]. $5 \times 10^5$ trajectories are run for each energy and initial rovibrational state. To select the initial conditions, the exact diatomic states of the reactants are obtained by solving the monodimensional Schrödinger equation to get the $E_{vj}$ eigenvalues and consider high rovibrational excitations. The classical turning points are then obtained for each individual initial vibrational state.

The reaction probability, $P_r^j(E)$, is calculated for selected total angular momentum, $J$, and each initial rotational state, $j$, of $H_2$. Batches of $10^5$ trajectories are run for each energy and $J$ value for a particular $(v, j)$ initial state. In this case the initial conditions are set with the following method:

1. First $J_z = j_z$ is set choosing a random number in the interval $[-min(j, J), min(j, J)]$. $J_x$ is set as a random number in the interval $[-(J-|J_z|), J-|J_z|]$. The absolute value of $J_y$ is then fixed and its sign is determined randomly.

2. The velocity vector is set along the $z$ axis is set as $\dot{\mathbf{R}}$ =(0,0, $v_R$), with $v_R = \sqrt{2\mu E}$.

3. $r = |\mathbf{r}|$ is set as one of the classical turning points of the initial state, selected randomly. Its polar angles $\theta_r, \phi_r$ are set by random numbers in the $[0, \pi]$ and $[0, 2\pi]$ intervals, respectively.

4. The velocity vector $\dot{\mathbf{r}}$ is set as

$$\begin{aligned}
(\dot{r})_x &= v_r \left(\cos\phi_r \cos\theta_r \cos\chi - \sin\phi_r \sin\chi\right) \\
(\dot{r})_y &= v_r \left(\sin\phi_r \cos\theta_r \cos\chi + \cos\phi_r \sin\chi\right) \\
(\dot{r})_z &= v_r \sin\theta_r \cos\chi,
\end{aligned}$$

with $v_r = j/(\mu_{BC} r)$, $\sin\chi = j_z/(j \sin\theta_r)$, $\mathbf{j} = \mu_{BC}\, \mathbf{r} \times \dot{\mathbf{r}}$ and $\mu_{BC} = m_B m_C/(m_B + m_C)$

5. The end-over-end angular momentum then becomes, **l**= **J** - **j**, and the impact parameter is $b = |\mathbf{l}|/(\mu v_R)$.

6. Finally the **R** vector is set as:

$$\begin{aligned}(\mathbf{R})_x &= b\sin\alpha \\ (\mathbf{R})_y &= b\cos\alpha \\ (\mathbf{R})_z &= \sqrt{R_0^2 - b^2} + \xi,\end{aligned}$$

with $\alpha = \arctan(-l_y/l_x)$ and $\xi$ a random number in the interval $\{0, Tv_R\}$. The period $T$ is the rovibrational period, which have to be determined precisely for a good sampling of the phase space. As the distribution of **r** is not isotropic in this case, the period is determined in two steps. We first estimate the vibrational and rotational periods as $T_v = 4\pi/(E_{v+1j} - E_{v-1j})$ and $T_j = \pi/(jB_v)$, respectively, where $B_v = \langle\Phi_v|\frac{\hbar^2}{2\mu_{BC}r^2}|\Phi_v\rangle$ is the rotational constant of the initial vibrational level $v$. Then, the Hamilton equations of motion of the diatomic molecule are integrated until $t_{max} = T_v + T_j$, and the rovibrational period $T$ is set as the time $t$ when the lowest $|\mathbf{r}(t) - \mathbf{r}(t=0)|$ distance is found. We should remark here that which such procedure, the obtained period T may differ significantly from the initial guess, specially for high (v,j) states.

### B. Quantum calculations

The quantum $H_2(v,j)$ + $S^+$ → $HS^+(v',j')$+ H state-to-state cross sections are calculated as

$$\sigma_{vj,v'j'}(E) = \frac{1}{2j+1}\sum_{\Omega,\Omega'}\sigma_{vj\Omega,v'j'\Omega'}(E), \qquad (3)$$

where $\Omega$ and $\Omega'$ are the projections of the total angular momentum vector, **J**, on the body-fixed z-axis of reactants and products Jacobi coordinates. The helicity dependent cross-section are defined as[17, 18]

$$\sigma_{vj\Omega,v'j'\Omega'} = \frac{\pi}{k_{vj}^2}\sum_{J\epsilon}(2J+1)\left|S^{J\epsilon}_{vj\Omega,v'j'\Omega'}\right|^2 \qquad (4)$$

with $k_{vj}^2 = 2\mu E/\hbar^2$ and $\mu = m_S m_{H_2}/(m_S + m_{H2})$. $J$ is the absolute value of the total angular momentum and $\epsilon$=±1 is the parity under inversion of coordinates. The reaction probability for each total angular momentum, $J$, and initial state, $v, j$, is defined as

$$P^J_{vj}(E) = \frac{2}{2j+1}\sum_{\Omega\Omega'}\sum_{v'j'\epsilon}\left|S^{J\epsilon}_{vj\Omega,v'j'\Omega'}(E)\right|^2. \qquad (5)$$

TABLE I: Parameters used in the wave packet calculations (all distances are given in Å).

| | |
|---|---|
| Scattering coordinate: | $R_{\min} = 0.001; R_{\max} = 34.0$ |
| Number of grid points in R: | 720 |
| Diatomic coordinate: | $r_{\min} = 0.1; r_{\max} = 34.0$ |
| Grid points in r : | 420 |
| No. of angular functions : | 320 |
| Initial wave packet position: | $R_0 = 20.0$ |
| Initial kinetic energy/eV : | $E_c = 0.8$ |
| Analysis distance: | $R_\infty$=10.0 |
| Chebyshev iterations: | 70000 |

The $S^{J\epsilon}_{vj\Omega,v'j'\Omega'}$ matrix elements are calculated with a quantum WP method for each value of $J, \epsilon$ and initial state quantum numbers $v, j, \Omega$. The MAD-WAVE3 program [19–21] has been used, using reactant Jacobi coordinates, and transforming to product Jacobi coordinates at each iteration as explained in Ref. [19]. The parameters used in the WP calculations are listed in Table I.

For $J = 0$ we also performed time-independent (TI) calculations with hyperspherical coordinates using the ABC code[22], with the parameters listed in Table II.

The helicity dependent cross section in Eq. (4) requires the summation over all the partial wave expansion up to $J = 70$ in this case, to get convergence up to 2 eV of translation energy. For this purpose we performed WP calculations for all $J$ in the interval $\Omega, 30$ for all the initial states $(v, j, \Omega)$ considered here. To save computational time, for $J > 30$, complete WP calculations were per-

TABLE II: Parameters used in the time-independent ABC calculations for total angular momentum quantum numbers $J = 0$ (distances are given in angstroms).

| | |
|---|---|
| Hypershperical maximal radius `rmax` | 45.0 |
| Number of grid points in r | 400 |
| Number of basis functions: | 491 |
| Maximum projection quantum number `kmax`: | 0 |
| Maximum rotational quantum number `jmax`: | 40 |
| Energy for basis cut/eV `emax` : | 4.0 |

formed only for some $J$ values, those multiple of 5. For intermediate $J$, $\left|S^{J\epsilon}_{vj\Omega,v'j'\Omega'}\right|^2$ matrix elements were calculated using the J-shifting interpolation method[12, 18].

## III. RESULTS AND DISCUSSION

### A. Potential energy surface

The PES of Ref. [11] has been used in all the calculations, and some minimum energy paths for several HHS angles are shown in Fig. 1. The reaction is endothermic by $\approx 0.95$ eV from $H_2(v = 0)$, with no barrier for a collinear configuration. As the HHS angle varies, a barrier for the reaction appears giving rise to a rather narrow cone of acceptance for the reaction to occur. For vibrationally excited $H_2$, $r$ is elongated and the internal energy increases, so that for $v$=2 the total energy is high enough to access $SH^+$ products. This was already investigated previously for this system using a QCT method[11], finding a considerable enhancement of the reactivity when increasing initial vibration.

### B. Effect of the initial states of reagents

The total integral cross section (ICS) for the $S^+$+$H_2(v, j) \rightarrow SH^+ + H$ reaction and different initial $v, j$ states of $H_2$ are shown in Fig. 2, obtained with

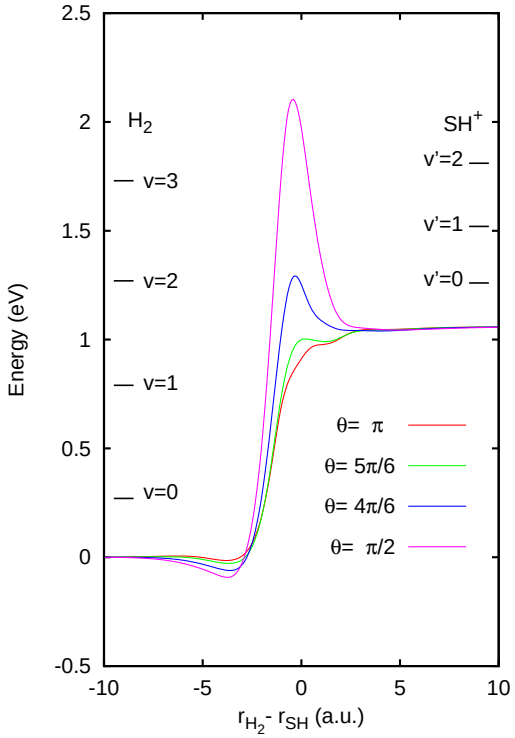


FIG. 1: Minimum energy path of the $S^+$+$H_2$ PES of Ref. [11] as a function of $r_{H_2} - r_{SH^+}$ difference for fixed $\angle HHS$ angle.

QCT and WP calculations. The ICS increases considerably with $v$, as it was reported prevously with QCT calculations[11]. Here, the effect of the initial rotational excitation is also reported and compared with quantum WP results. It is found that the reaction ICS increases also when increasing the rotation excitation, specially from $j$=0 to 1. This effect is found in QCT and WP results, but for $j$=0 the QCT ones understimate considerably the ICS, for both $v = 2$ and $v = 3$

The increase of the ICS with the initial vibrational excitation, $v$, is well understood. The vibrational excitation brings energy in the mode associated to the reaction coordinate that have to be broken in order to form the $SH^+$ product. Additionally, the energy for $v \geq 2$ is sufficient for the reaction to become exothermic. The effect of rotation is more surprising, specially because a significant

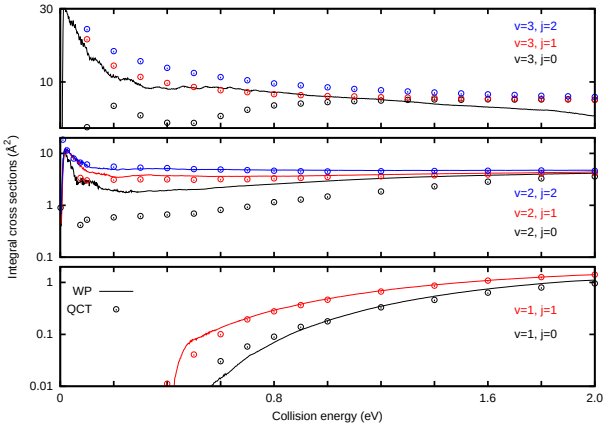


FIG. 2: Integral cross section for the $S^+ + H_2(v, j) \rightarrow SH^+ + H$ reaction as a function of the collision energy, for different initial states of $H_2$, $v = 1, j = 0, 1$ (bottom panel), $v = 2, j = 0, 1, 2$ (middle panel) and $v = 3, j = 0, 1, 2$ (top panel), and indicated in the figure. Open circles correspond to QCT calculations and lines to quantum WP results. In the case $v = 3$, quantum calculations were only performed for $j = 0$.

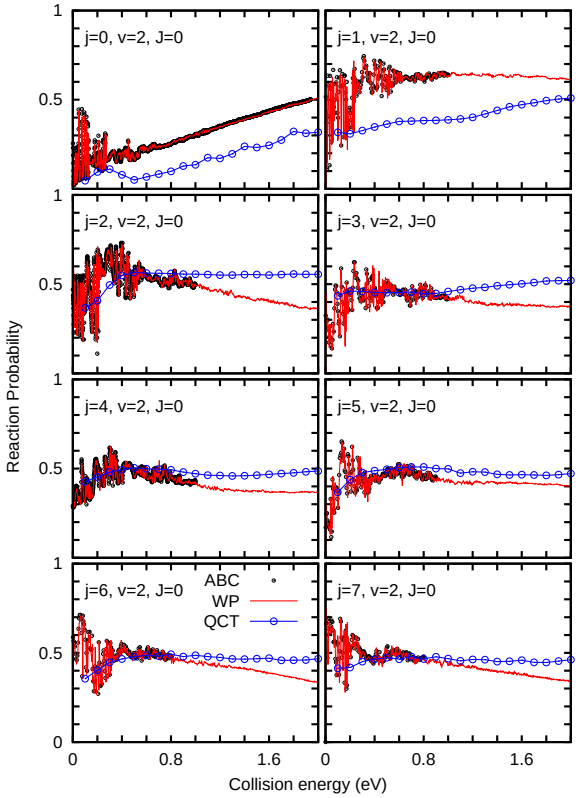


FIG. 3: Reaction probabilities for $S^+ + H_2(v = 2, j)$ as a function of collision energy for zero total angular momentum, $J = 0$, and different initial rotational states, as indicated in each panel.

difference is observed between QCT and WP calculations for $j$=0, in the cases of $v = 2$ and 3.

To understand the effect of the rotation, calculations for zero total angular momentum, $J = 0$, have been performed for several initial rotational states $j$ and $v = 2$, shown in Fig. 3. In order to assess the convergence of quantum results, TI calculations were performed giving results in very good agreement with the WP ones. The QCT results for $j$=0 and $j$=1 are considerably lower than the quantum ones. However, for higher $j$'s the agreement improve.

The effect of the total angular momentum, $J$, on quantum and classical results can be seen in the opacity functions shown in Fig. 4 for several initial states of $H_2$. For $v = 2, j = 0$, the QCT probabilities are always lower than the WP results. For $v = 2, j = 1$ the QCT results are only lower for $J < 30$ while for $v = 2, j = 2$, QCT and WP results are in good agreement. Thus, high end-over-end angular momentum, $\ell$, seems to increase the QCT reactivity, providing results in better aggreement with the WP ones. For $v = 3, j = 0$, the reactivity for $j = 0$ is already relatively high, so that QCT and WP agree for $J > 30$.

These results indicates that in a QCT treatment, the system needs more rotational excitation to react, and that it is more effective when the $H_2$ rotation is excited.

In order to go deeper inside the dynamics, the stereodynamics is analyzed and in Fig. 5 the helicity dependent cross section is shown for $v = 2, j = 1$ and 2. $\Omega$ is the projection of $\mathbf{j}$ on the z-axis, parallel to $\mathbf{R}$, and $\Omega = 0$ for $j > 0$ corresponds to an angular distribution with a maximum at collinear configurations, while $\Omega = \pm j$ is a

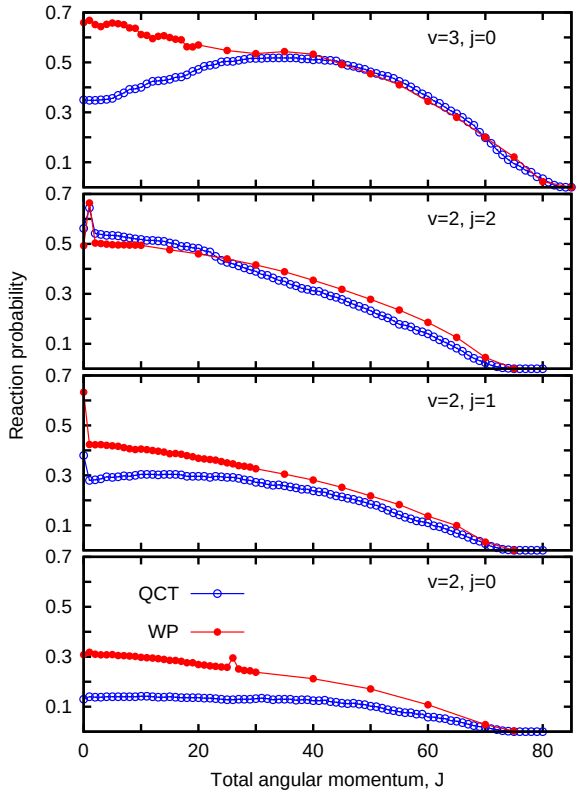


FIG. 4: Reaction probability as a function of total angular momentum, $J$, for a collision energy of 1 eV and different initial states of $H_2$, as indicated in each panel. Open circles are QCT resuls, while closed circles are the quantum WP ones.

T-shaped configuration. Assuming that the orientation of **j** do not change significantly in the entrance channel, $\sigma_{\Omega=0} > \sigma_{\Omega=j}$ indicates that the reaction is favoured for collinear approaches as discussed previously[18, 23, 24]. For $j = 1$, this is the case for low energies, $E < 0.8$ eV . For higher energies, the angular cone of acceptance increases, and the dependence of the reactivity on the relative orientation decreases. For $j = 2$ this is also the case, but the dependence is less marked.

Additionally, QCT calculations were performed fixing the initial orientation to collinear or T-shaped configurations for several energies and $v = 2, j = 0$. It is found that the cross section is considerably larger for

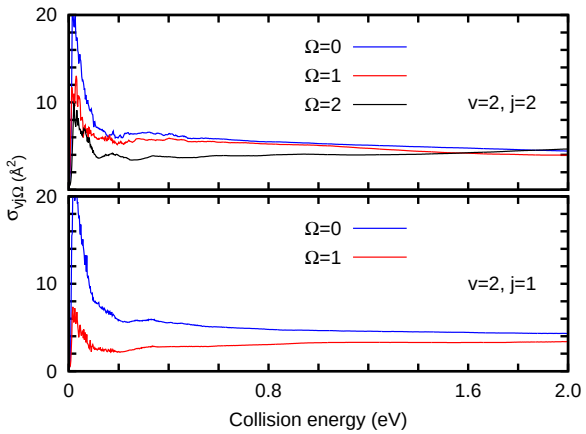


FIG. 5: Quantum WP total helicity dependent cross section (obtained from Eq. (3) by summing over all final states of products) for $v = 2, j = 1$ and 2.

the trajectories starting at collinear configurations as compared to those starting at T-shaped configurations. Moreover, when setting the impact parameter to zero, $b = 0 \equiv J = 0$, the trajectories starting at T-shaped configurations showed a very small reaction probability, nearly negligible.

All these results lead us to make a simple model for the reaction dynamics in this system. The PES in the entrance channel is rather isotropic so that for $j = 0$ and $J = 0$ the orientation between the two reagents do not vary significantly in the entrance channel. Since a higher barrier is present at bent geometries, see Fig. 1, the reactivity is strongly enhanced for those trajectories starting at collinear configurations. As the angular momenta increase, the system rotate during the approach of the two reactants, leading them the opportunity of finding the channel towards products.

This explains not only the important enhancement of the reactivity with increasing initial rotation but also the differences appearing between QCT and WP calculations. In the QCT method, each trajectory samples its

own path without exploring other regions of the configuration space. However, the wave packet is non local, and is delocalized in the angular coordinates, thus exploring collinear as well as T-hsaped configurations at once. This makes that for $j = 0, J = 0$ the wave packet leads to a higher reactivity than the classical trajectories.

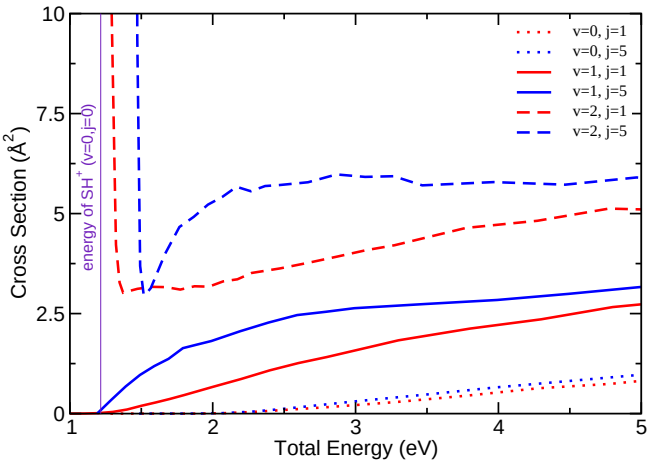


FIG. 6: Total reaction cross section for several rovibrational states as a function of total energy.

Since rovibrational excitation has a significant effect, it is interesting to quantify this effect when vibrational and rotational quantum numbers $v$ and $j$ increase. In order to analyse this effect, QCT calculations were performed for several initial rovibrational states of $H_2$(v=0,1,2; j=1,5), shown in Fig. 6. As it can be seen, both vibrational and rotational excitations provide a considerable enhancement of the reactivity for a given total energy, while collision energy is found to be much less efficient. It is also interesting to see that the enhancement of reactivity due to rotation increases when the vibrational excitation is bigger. For $v = 0$, the augmentation of the cross section is rather moderate when the $j$ varies from 1 to 5, and the cross section starts to increase at energies far beyond the opening of the $SH^+$ channel. For $v = 1$ however, the augmentation observed between $j = 1$ and $j = 5$ is considerable and for $v = 2$, the effect seems to grow even stronger.

It is interesting to point out that for this system, the distribution of the energy in the different modes can change significantly the reactivity. This indicates that energy is not effectively transferred from a mode to another. In order to quantify the influence of vibrational and rotational energy contribution on reactivity, and have a better insight on energy transfers, collisions of $S^+$ with $H_2$ in several rovibrational states with approximately the same internal energy have been performed. The benchmark was set to $H_2(v = 3, j = 1)$, for which reaction exothermicity is 0.5 eV. To obtain the approximately the same internal energy for the comparison, the appropriate rotational levels have been choosen for lower vibrational numbers, which are $(v = 2, j = 8)$, $(v = 1, j = 12)$ and $(v = 0, j = 15)$. The results for collisions energies up to 2 eV are shown in Fig. 7.

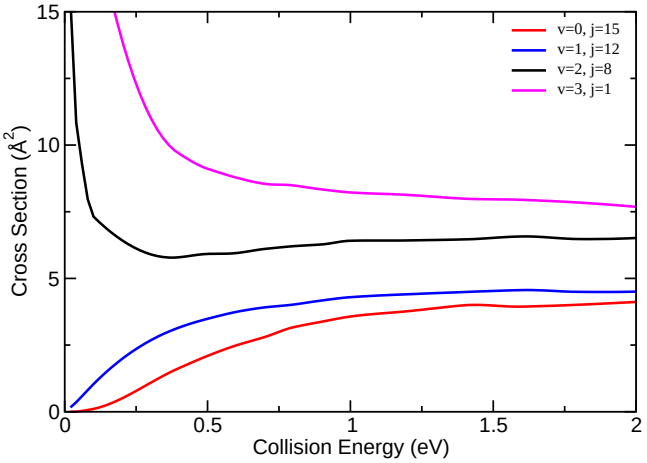


FIG. 7: Total reaction cross section for several rovibrational states of similar internal energy as a function of collison energy.

As it can be seen, even with $H_2$ having similar internal energy, the cross sections as a function of collision energy exhibits very different behaviour. The first observation is that vibrational energy is the more favorable to reactivity. As mentioned before, it is the mode that has to be activated to obtain reaction. The second observation is that there is a clear trend difference between vibrational states that are endothermic when $j = 0$ $(v = 0, 1)$, for which cross section decrease to nearly zero at low colli-

sion energy while the exothermic ones ($v = 2, 3$) exhibit an important increase in the cross section at low collision energy behaving like typical barrierless exothermic reactions. Similar behaviour is also seen in Fig. 6. This difference is striking, as in all the cases, the reaction is exothermic and does not present any barriers. This confirms that the energy transfer between rotation and vibration is not effective, specially at low collision energies. As a consequence the reaction probability decreases significantly when collision energy become small for v=0 and 1, while there is always a probability to react when v>1. This leads to high cross sections for v>1 since at low collision energy the trajectories are deviated toward the well in the entrance channel leading to an increase of the impact parameter with decreasing energy. On the contrary, for v=0 and 1, cross section drops because the probability to react tends to zero.

The inefficiency of energy transfer in this system can be understood considering that the potential does not present a deep well allowing the formation of a stable complex. This implies that the important rotational effect on reactivity is not associated to the increase of energy, but rather to a major exploration of the PES, enhancing the probability to find the path towards products. This can also explain why the rotational excitation is more favorable to reactivity for higher vibrational levels. By providing a better exploration of the PES, the effect of rotation is thus magnified when the cone of acceptance is bigger, providing an interesting synergic effect of the rovibrational excitation for this reaction.

This result has important implications in astrochemistry. First of all, a significant difference of reactivity is expected between *ortho* and *para* hydrogen. Additionally, as the density of molecules is low in the ISM, molecules like $H_2$ do not thermalise efficiently, and in particular in highly irradiated regions like PDR where rovibrational exctiation can be achieved by photon absorption. In this case, in order to modelize correctly the formation of $SH^+$, it is necessary to consider state-to-state rate constants because of the important effects of rovibrational excitation.

### C. Resonances and roaming trajectories

The WP reaction probabilities, in Fig. 3, show resonant structures for collisional energies below 1 eV for all the $j$'s studied. Since the PES only presents a very shallow well in the entrance channel, the apparition of this resonant behaviour is surprising, and needs to be analysized. The QCT reaction probabilities does not show such behaviour. However, when the collision time is analyzed, many long lived trajectories occurs at these relatively low collision energies. Typical examples of such long lived trajectories are depicted in Fig. 8. These trajectories clearly show that after a first impact, the $H_2$ rotation gets excited (we remind that vibrational excitation is very inefficient in our system), and the remaining translation energy becomes to small to yield to dissociation. Thus, after reaching the outer classical turning point, the system flies back to collide again, and this process is repeated until the system gets enough translation energy to dissociate, either in the entrance or the product channels. These kind of trajectories can be classified as roaming trajectories[25–27]. Recently, such trajectories were found in triatomic systems, in the dynamics of the MgH+H reaction[28, 29].

In order to establish the link between these roaming trajectories and the quantum resonances we need to determine how important are these trajectories and what is their effect on reaction probabilities. The roaming probabilities, shown in top panel of Fig. 9 in the case of $H_2$ (v=2,j=1) for J=0 and 10, clearly increases at low collision energy. This roaming probability is defined as the ratio between the number of roaming trajectories and the total number of trajectories, roaming trajectories being defined in a first approximation as those having a residence lifetime superior twice the average value at the same total energy. In the bottom panel of Fig. 9, reaction

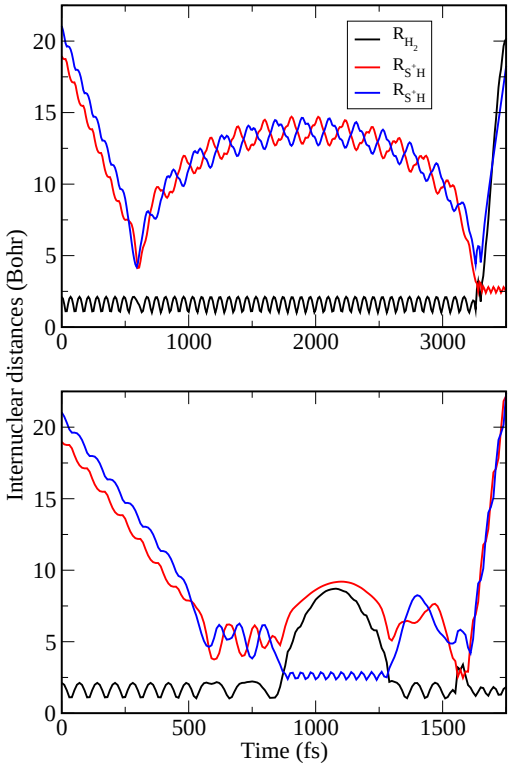


FIG. 8: Evolution of the internuclear distances as function or propagation time for two typical roaming trajectories.

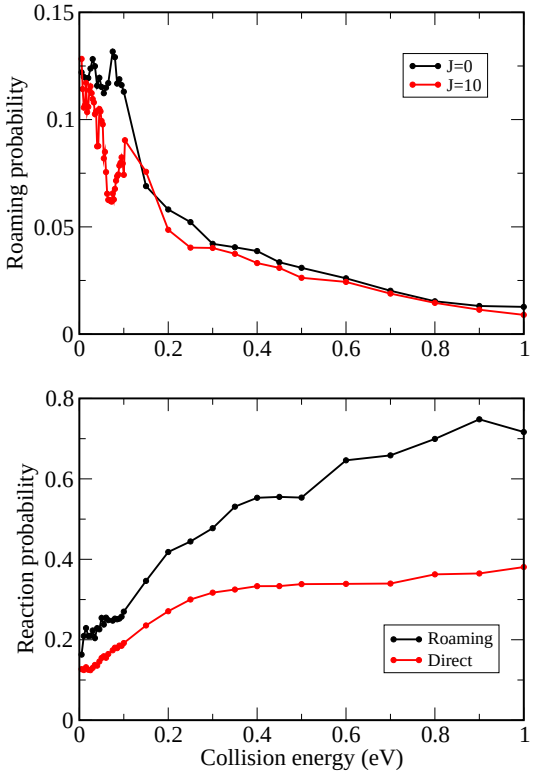


FIG. 9: Probability to obtain roaming trajectories as a function of collision energy for $H_2$ ($v = 2, j = 1$) when impact parameter is set to J=0 and 10 (top panel), and reaction probability of both direct and roaming trajectories in the case J=0.

probabilities of direct and roaming trajectories are ploted (J=0). As expected, it appears clearly that roaming trajectories are more reactive than direct ones as the rotation of $H_2$ is excited at the first impact, favouring reactivity. Since the probability to obtain roaming as function of energy match the range where quantum resonances appear and considering the enhancement of reactivity of these trajectories, we can conclude that the quantum resonances can be associated to a quantum manifestation of roaming trajectories.

According to Mauguière *et al.*, roaming occure only in well defined roaming regions of the phase space clearly separated from non roaming regions, in which both reactive and inelastic trajectories are trapped for an arbitrarily long time[30]. In a quantum approach, all regions of the phase space are sampled at once, including regions associated with roaming trajectories, giving rise to a resolved resonant structure. However, in the global QCT probabilities, these resonances cannot be observed because the Monte Carlo procedure provide an average value over all the phase space. This is not always the case. If the roaming regions are dense enough in the phase space, resonances may appear classicaly as reported in ref. [31], where classical resonances mimicking the quantum ones have been observed for J=0 at collision energy near the threshold.

### D. State-to-state results

The quantum vibrationally resolved state-to-state cross sections obtained for several initial states are shown in Fig. 10. For initial $v = 2$ and $E < 0.8$ eV, the final vibrational distributions of $SH^+(v')$ states is reduced to only $v' = 0$, with a minor contribution from more excited states. As for exothermic reactions, the cross section decreases with increasing the collision energy, and the cross section at low energy increases with $v$, as discussed below. At higher energies, $E > 1.6$ eV, the cross section for $v' = 0$ is still the highest but comparable to those of $v'$= 1, 2 and 3, and all of them rather small, $\approx 2$ Å$^2$.

For initial $v = 3, j = 0$, the final vibrational distribution of $SH^+$ products correspond to a nearly equal proportion of $v' = 0$ and 1. These two final states present the highest cross sections for $E < 0.4$ eV, while for $E > 0.8$ eV all final vibrational states present nearly the same cross sections. As the potential does not present any barriers in the exit channel, once the system reaches this region, it can be considered that it will not come back. An analogy with the case of late barrier reactions can thus be established and the Polanyi rules can be applied [32, 33]. Vibrational excitation of reactants will favorise the reactivity leading to higher cross sections and the collision energy will be preferentially deposited as vibrational energy of the products.

The state-to-state cross section to each individual rotational state, $j'$, of $SH^+$ products are shown in Figs. 11 and 12 for collisions starting in $v = 2, j = 0$ and $v = 3, j = 0$, respectively. For collisions starting in $v$=2, $j$=0, the highest rotationally resolved cross sections are found at low collision energy for relatively low $j'$ values, the maximum being obtain for $j' = 3$. When increasing collision energy and $j'$ the cross section decreases smoothly. Similar behaviour are found for $j$ =1, 2 and 3.

The rotationally resolved cross section for $v$=3, $j$=0 are rather different to those of $v$=2. For $v = 3$ there is more available energy making possible to form $SH^+$ products in vibrational levels $v'$=0 and 1. The highest cross sections are also found at low energy, but the rotational levels with the highest cross sections are found to be $j'$= 15 and 7 for $v'$=0 and 1, respectively. These values are considerably higher than the one obtain for $v = 2, j = 0$, where the maximum was found for $j'$=3.

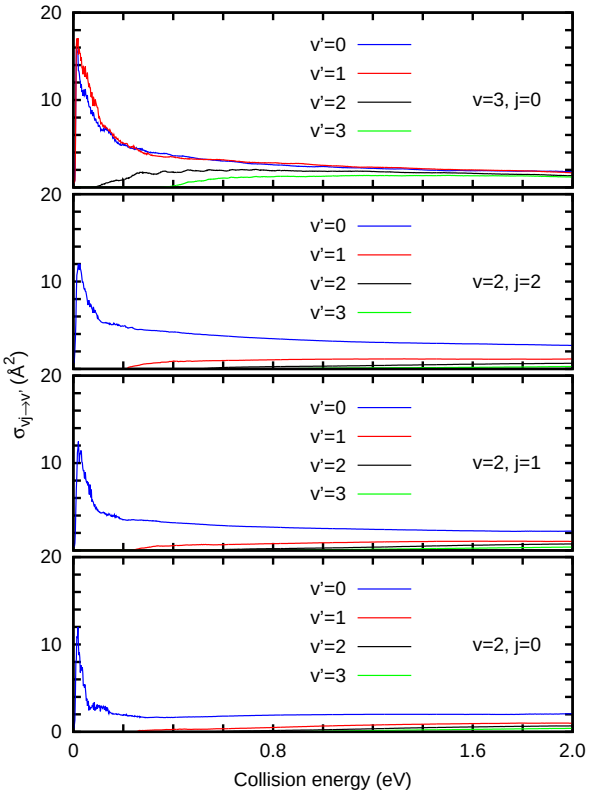


FIG. 10: Final vibrational cross section for the $H_2(v, j)$ + $S^+$ → $SH^+$ + ($v'$)+H collisions obtained with the WP method for $v$=2, $j$=0,1,2 and $v$=3,$j$=0, as indicated in the corresponding panel.

The quantum WP computational cost increases with $j$, since $(2j+1)$ calculations have to be performed (one per initial Ω value). Thus, this kind of calculations becomes prohibitive for high $j$. For this purpose QCT calculations could be well adapted. Since the QCT cross sections obtained for $j = 0$ and 1 are in general too low as compared

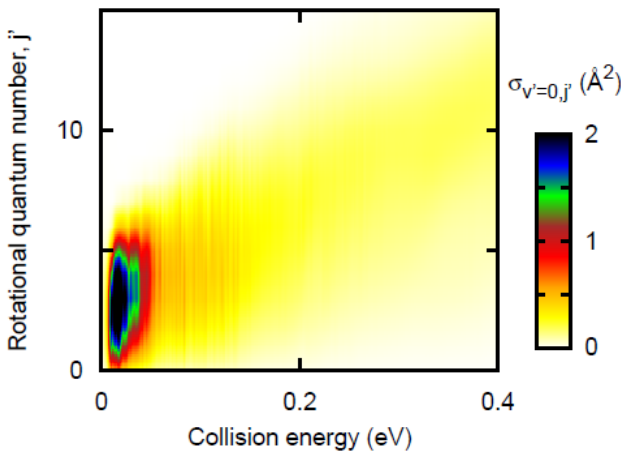


FIG. 11: WP state-to-state cross section for the $H_2(v=2, j=0) + S^+ \rightarrow SH^+ + (v'=0, j')$+H reaction as a function of collision energy.

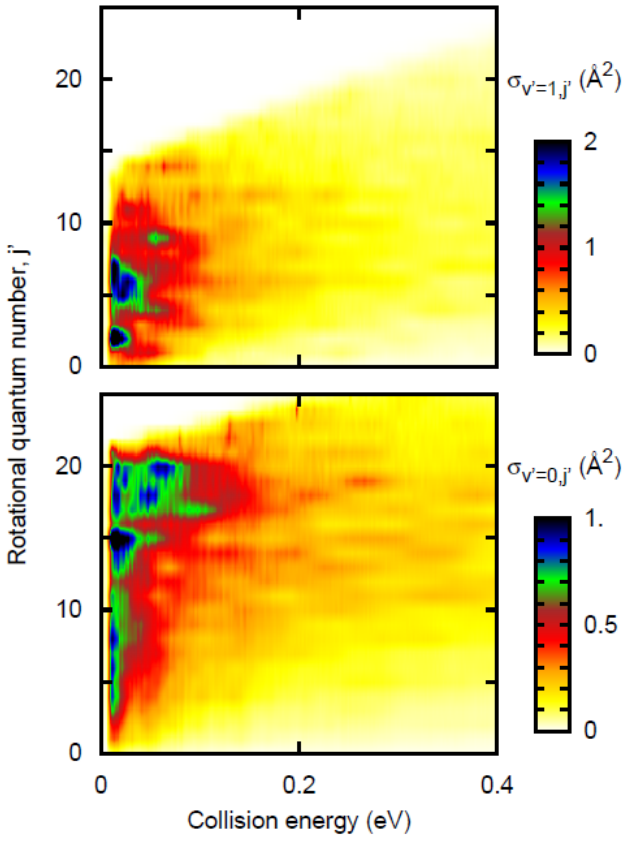


FIG. 12: WP state-to-state cross section for the $H_2(v=3, j=0) + S^+ \rightarrow SH^+ + (v', j')$+H reaction as a function of collision energy. Bottom panel correspond to $v'=0$, and top panel to $v'=1$

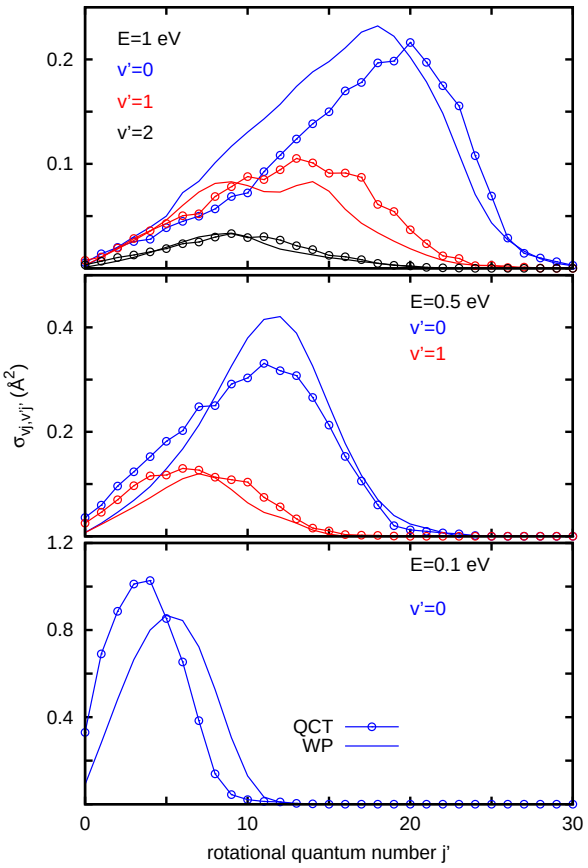


FIG. 13: QCT and WP state-to-state cross section for $H_2(v=2, j=2) + S^+ \rightarrow SH^+ + (v', j')$+H collisions as a function of $j'$ at fixed collision energies, 1.0, 0.5 and 0.1 eV for the top, middle and bottom panels respectively.

with the WP ones, it is worth trying to analyze how good QCT calculations are for determining state-to-state cross sections for $v=2, j=2$ a moderate $j$ for which the total reaction cross section works fairly well. In Fig. 13 the WP and QCT results are compared at three collision energies. In the three cases and for all the final vibrational states, $v'$, considered the agreement is rather good. In the present case the discretization of the quantum numbers has been done with the most common histogram binning. These results can be taken as an indication that to consider higher rotational excitations of the reactants, the QCT method would yield reasonably good results.

### E. Comparison with experimental results

In order to get a better idea of the quality of the potential, and to check the consequence of an adiabatic treatment discarding spin-orbit couplings, QCT calculations were performed for $S^+$+HD and $S^+$+$D_2$ to reproduce the experimental results published by Stowe *et al.*[1]. It is interesting to point out that in the case of $D_2$, a spin orbit contribution to the cross section have been estimated experimentally showing an important effect of the intersystem crossing between the $^4A''$ state and the $^2A''$, both leading to $SH^+(^3\Sigma^-)$+$H(^2S)$ as can be seen in Fig. 4 of Ref. [1]. In the case of HD, no spin-orbit contributions were reported. As the experiment was done at 300K, the initial conditions were chosen for a thermalized rovibrational population, and calculation were done for collisions energies up to 15 eV. In order to compare our results, the experimental results were extracted graphically, and the spin-orbit contribution have been substracted to the experimental value. The experimental and calculated cross section for HD and $D_2$ as a function of collision energy are shown in Fig. 14.

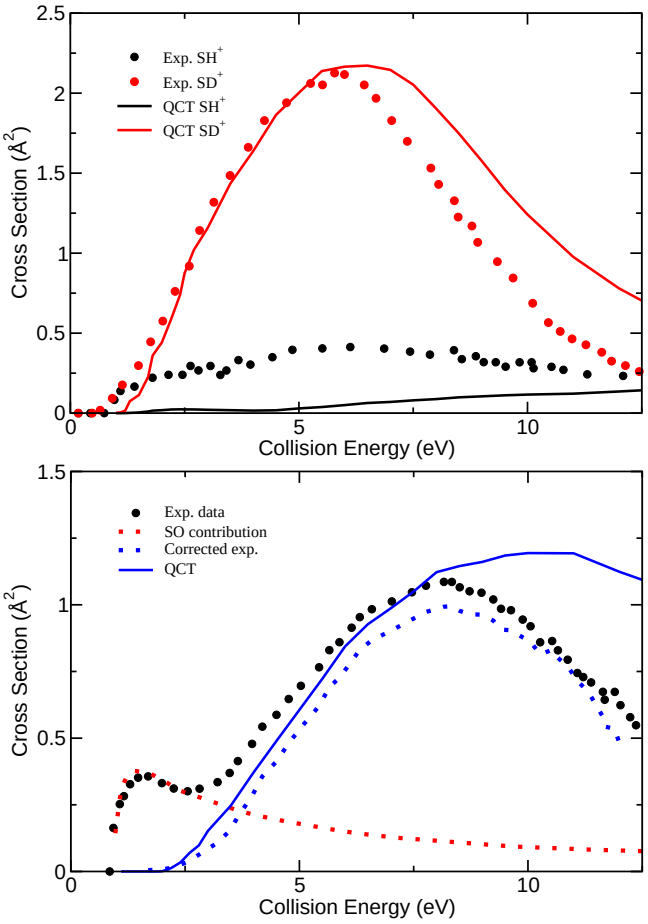


FIG. 14: QCT (solid line) and experimental (points) cross section for collision of $S^+$ with HD (top) and $D_2$ (bottom). For $D_2$, the experimentally evaluated spin-orbit contribution (red dots) have been substracted from the total experimental results (black points) to get the corrected experimental results (blue dots).

The global behaviour of calculated results and experimental results is very similar. In the case of $D_2$, the calculated cross section lies between the absolute experimental cross section and the corrected one. Considering that the spin orbit contribution is an estimation, we can consider the agreement as satisfactory, at least for energies lower than the experimental maximum.

In the case of HD, both calculations and experiment show that the production of $SD^+$ is dominant. Additionally, the agreement obtained is very good for the cross section associated to the formation of $SD^+$. However the calculated QCT cross section for the $SH^+$ channel is largely underestimated compared to the experimental one. As no spin-orbit effect have been reported in the experimental work and the spin-orbit contribution is clear for $D_2$, it is legitimate to think that the formation of $SH^+$ in the case of HD is dominated by the spin-orbit contribution while the formation of $SD^+$ is dominated by the adiabatic reaction on the quartet state, as suggested by the good agreement between theory and experiment. If the interpretation is correct, this effect would be quite interesting, but calculations including the different spin-orbit states and their couplings will be necessary. Considering the experimental result with $D_2$, taking in account spin-orbit contribution seems also important in order to study the reactivity to confirm and understand this hypothesis. As this contribution is stronger at lower collision energy,

estimating this effect for very low collision energy and high vibrational level may be very interesting as an increase in the cross section at low energy will have an important effect on the calculated rate constants.

Another interesting point to note is that a maximum in the cross sections is observed experimentally for both HD and $D_2$ at 6 eV and 8 eV respectively. This maximum is associated to the total dissociation ($S^+$+H+H) which becomes dominant at high collisions energy leading to a collapse of the probability to form $SH^+$[34]. This maximum is also observed in the calculations, were the maximum in cross section found for HD is found at lower energy than the maximum obtained with $D_2$. However, the calculated maxima are found at higher energies that the one found in the experiment. The discrepancy probably comes from the lack of precision of repulsive part of the potential at very high energy as it was not optimized to describe accurately this region in this work. The difference in the position of the maxima can be explained by the difference in the isotropy of the repulsive potential. Indeed, in Ref. [14], it was shown that a bigger anisotropy of the repulsive potential was favouring the total dissociation mechanism. By changing the position of the center of mass, the anisotropy of the potential increases in the case of HD, making the total dissociation mechanism more favorable than in the case of $D_2$. As a consequence, the hydride formation cross sections drop faster for HD, and the maximum appears at lower collision energy.

## IV. CONCLUSIONS

In this work, a detailed study of the effect of rovibrational excitation on the reaction between $S^+$+$H_2$ is done by performing WP and QCT dynamical calculations on the quartet state *ab initio* PES developed by Zanchet *et al*[11]. It is found that for $j = 0$, QCT method is unable to reproduce WP results, but a good agreement is found between the two methods for higher rotational levels. To get a better insight on the reaction, stereodynamics study is also performed. As a result of our calculations, it is found that vibrational energy is the more favorable to the formation of the $SH^+$ product. Rotational excitation is also found to have an important effect on reactivity by providing a better exploration of the PES during the reaction and increasing the probability to find a path toward the products. Additionally, a synergy is observed between the vibrational and the rotational excitation, leading to a major effect of the rotation when the vibrational energy is higher. In this context, the reactivity strongly depends on the rovibrational state of $H_2$. This effect of rotation have an additional indirect consequence leading to the presence of resonances in the WP calculations. They are explain by a roaming mechanism which implies a rotational excitation of $H_2$ after a first impact, trapping the system for a while before a second impact with $H_2$ rotationally excited. Roaming mechanism thus present an enhanced reaction probability compared to the direct one. This reaction being important from an astrochemical point of view, as it is one of the route to form $SH^+$, it is necessary to provide state-to-state data to consider this reaction properly. In this scope, we present in this work the first state-to-state and state-to-all accurate WP reaction cross sections for $S^+$+$H_2(v, j)$ for $(v = 2, j = 0, 1, 2)$ and $(v = 3, j = 0)$. Finally, a comparison with the experimental data published by Stowe *et al.* [1] exhibits satifactory agreement for the contribution of the quartet state considered in this work, but demonstrate the necessity to take in account spin-orbit couplings to get a better description of this reaction.

## V. ACKNOWLEDGEMENTS

O.R. and N.B. acknowledge CSIC for travelling grant I-LINK0775. Financial support from the Scientific and Technological Research Council of TURKEY (TUBITAK) (Project No. TBAG-112T827) and from the Ministerio de Economía e Innovación (Spain), for grants

CSD2009-00038 and FIS2014-52172-C2 are gratefully acknowledged. The computations have been performed on the High Performance and Grid Computing Center (TR-Grid) at ULAKBIM/TURKEY and CESGA computer center. We also thank the support from the European Research Council under the European Union's Seventh Framework Programme (FP/2007-2013) / ERC Grant Agreement n. 610256 (NANOCOSMOS). We also acknowledge the COST action CM1401 'Our Astrochemical History'.

## VI. REFERENCES

[1] G. F. Stowe, R. H. Schultz, C. A. Wright, and P. B. Armentrout, Int. J. Mass Spectrom. Ion Proc. **100**, 377 (1990).

[2] M. Agúndez and V. Wakelam, Chem. Rev. **113**, 8710 (2013).

[3] D. E. Anderson, E. A. Bergin, S. Maret, and V. Wakelam, Astrophys. J. **779**, 141 (2013).

[4] A. O. Benz, S. Bruderer, E. F. van Dishoeck, P. Stuber, S. F. Wampfler, M. Melchior, C. Dedes, F. Wyrowski, S. D. Doty, F. van der Tak, et al., Astron. Astrophys. **521**, L35 (2010).

[5] K. M. Menten, F. Wyrowski, A. Belloche, R. Güsten, L. Dedes, and H. S. P. Müller, Astron. Astrophys. **525**, A77 (2011).

[6] B. Godard, E. Falgarone, M. Gerin, D. C.Lis, M. De Luca, J. H. Black, J. R. Goicoechea, J. Cernicharo, D. A. Neufeld, K. M. Menten, et al., Astrophys. J. **540**, 87 (2012).

[7] Z. Nagy, F. F. S. V. der Tak, V. Ossenkopf, M. Gerin, F. L. Petit, J. L. Bourlot, J. H. Black, J. R. Goicoechea, C. Joblin, M. Rllig, et al., Astron. Astrophys. **550**, A96 (2013).

[8] D. T. Halfen and L. Ziurys, Astrophys. J. **814**, 119 (2015).

[9] T. J. Millar, N. G. Adams, D. Smith, W. Lindinger, and H. Villinger, MNRAS **221**, 673 (1986).

[10] M. Agúndez, J. R. Goicoechea, J. Cernicharo, A. Faure, and E. Roueff, Astrophys. J. **713**, 662 (2010).

[11] A. Zanchet, M. Agúndez, V. J. Herrero, A. Aguado, and O. Roncero, The Astronomical Journal **146**, 125 (2013), URL `http://stacks.iop.org/1538-3881/146/i=5/a=125`.

[12] A. Zanchet, B. Godard, N. Bulut, O. Roncero, P. Halvick, and J. Cernicharo, Astrophys. J. **766**, 80 (2013).

[13] S. Gómez-Carrasco, B. Godard, F. Lique, N. Bulut, J. Klos, O. Roncero, A. Aguado, F. J. Aoiz, M. E. J. F. Castillo, J. R. Goicoechea, and J. Cernicharo, Astrophys. J. **794**, 33 (2014).

[14] A. Dorta-Urra, A.Zanchet, O. Roncero, and A. Aguado, J. Chem. Phys. **142**, 154301 (2015).

[15] L. F. Shampine and M. K. Gordon, DDEABM is a driver for a modification of the code ODE written by L. F. Shampine and M. K. Gordon Sandia Laboratories Albuquerque, New Mexico 87185.

[16] M. Karplus, R. N. Porter, and R. D. Sharma, J. Chem. Phys. **43**, 3259 (1965).

[17] A. Aguado, M. Paniagua, M. Lara, and O. Roncero, J. Chem. Phys. **107**, 10085 (1997).

[18] M. Lara, A. Aguado, O. Roncero, and M. Paniagua, J. Chem. Phys. **109**, 9391 (1998).

[19] S. Gómez-Carrasco and O. Roncero, J. Chem. Phys. **125**, 054102 (2006).

[20] A. Zanchet, O. Roncero, T. González-Lezana, A. Rodríguez-López, A. Aguado, C. Sanz-Sanz, and S. Gómez-Carrasco, J. Phys. Chem. A **113**, 14488 (2009).

[21] A. Zanchet, T. González-Lezana, A. Aguado, S. Gómez-Carrasco, and O. Roncero, J. Phys. Chem. A **114**, 9733 (2010).

[22] D. Skouteris, J. Castillo, and D. E. Manolopoulos, Comp. Phys. Commun. **133**, 128 (2000).

[23] L. González-Sánchez, S. Gómez-Carrasco, A. Aguado, M. Paniagua, M. L. Hernández, J. M. Alvariño, and O. Roncero, Mol. Phys. **102**, 2381 (2004).

[24] L. González-Sánchez, O. Vasyutinskii, A. Zanchet, C. Sanz-Sanz, and O. Roncero, Phys. Chem. Chem. Phys. **13**, 13656 (2011).

[25] D. Townsend, S. A. Lahankar, S. K. Lee, S. D. Chambreau, A. G. Suits, X. Zhang, J. Rheinecker, L. B. Harding, and J. M. Bowman, Science **306**, 1158 (2004).

[26] J. M. Bowman and B. C. Shepler, Annu. Rev. Phys. Chem. **62**, 531 (2011).

[27] J. M. Bowman, Mol. Phys. **112**, 2516 (2014).

[28] T. Takanayagi and T. Tanaka, Chem. Phys. Lett. **504**, 130 (2011).

[29] A. Li, J. Li, and H. Guo, J. Phys. Chem. A **117**, 5052 (2013).

[30] F. A. I. Mauguière, P. C. amd G. S. Ezra, S. C. Farantos, and S. Wiggins, Chem. Phys. Lett. **592**, 282 (2014).

[31] S. Gómez-Carrasco, L. González-Sánchez, A. Aguado, O. Roncero, J. M. Alvariño, M. L. Hernández, and M. Paniagua, J. Chem. Phys. , **121**, 4605 (2004).

[32] J. Polanyi and W. Wong, J. Chem. Phys. **51**, 1439 (1969).

[33] M. Mok and J. C. Polanyi, J. Chem. Phys. **51**, 1451 (1969).

[34] A. Dorta-Urra, A. Zanchet, O. Roncero, A. Aguado, and P. B. Armentrout, J. Chem. Phys. **135**, 091102 (2011).